

Battery Health-conscious Plug-in Hybrid Electric Vehicle Grid Demand Prediction

Saeid Bashash

Department of Mechanical Engineering
University of Michigan
Ann Arbor, MI 48109
bashash@umich.edu

Scott J. Moura

Department of Mechanical Engineering
University of Michigan
Ann Arbor, MI 48109
sjmoura@umich.edu

Hosam K. Fathy¹

Department of Mechanical Engineering
University of Michigan
Ann Arbor, MI 48109
hfathy@umich.edu

ABSTRACT

This paper examines the problem of predicting the aggregate grid load imposed by battery health-conscious plug-in hybrid electric vehicle (PHEV) charging. The paper begins by generating a set of representative daily PHEV trips using the National Household Travel Survey (NHTS) and a set of federal and real-world drive cycles. Each trip is then used in a multiobjective genetic optimizer, along with a PHEV model and a battery degradation model, to simultaneously minimize PHEV energy cost and battery degradation. The optimization variables include the parameters of the PHEV charge pattern, defined as the timing and rate with which the PHEV receives electricity from the grid. For several weightings of the optimization objectives, total PHEV power demand is predicted by accumulating the charge patterns for individual PHEVs. Two charging scenarios, i.e., charging at home only versus charging at home and work, are examined. Results indicate that the main PHEV peak load occurs early in the morning (between 5.00-6.00a.m.), with approximately 45%- 60% of vehicles simultaneously charging from the grid. Moreover, charging at work creates additional peaks in this load pattern.

1. INTRODUCTION

A large worldwide market penetration is envisioned for PHEVs within the next few decades. Due to their high energy demand, PHEVs will introduce a growing electric load to the regional power grids [1, 2]. Therefore, the prediction of PHEV

power demand is a necessity for the electric utility infrastructure to expand accordingly. Such prediction, however, requires information on the penetration, driving schedule, and charging pattern of PHEVs.

The literature on the PHEV powertrain system design, power management, and interaction with power grid is still at an incipient stage. A market share of about 25% is projected in the United States by year 2020, resulting in nearly five million PHEV sales per year [2]. The energy requirements of PHEVs depend significantly on the vehicle dynamics specifications (such as vehicle mass and the aerodynamic coefficient), battery size [3], powertrain configuration (e.g., series, parallel, and power-split [4]), power management strategy (e.g., blended versus charge-depletion charge-sustenance (CDCS) [3, 5]), and the driving behavior of PHEV owners. There are also studies on the vehicle-to-grid (V2G) integration and the effects of pricing policy on the charging characteristics of PHEVs [6-10]. However, the literature on battery health degradation from the V2G standpoint is scarce [11, 12]. The importance of battery health-conscious PHEV power demand prediction stems from the fact that battery degradation can play a key role in determining the optimal charging schedule of PHEVs [12].

Recent research by the authors examined the problem of optimizing the charge pattern for a single PHEV to improve its total daily energy cost and battery longevity [12]. This study

¹ Corresponding author.

showed that the optimal charge pattern for a PHEV depends significantly on the interplay between trip length, trip timing, and electricity pricing. The study modeled battery health degradation using a high-fidelity electrochemistry-based model [13-15] of Lithium-ion batteries. Accounting for battery health using this model resulted in optimal charge patterns that shift charging as close as possible to trip initiation (i.e., departure time). These patterns contrast considerably with the more traditional *late-afternoon* and *overnight* patterns examined in earlier research.

This paper extends the above research by optimizing the charge pattern for a number of PHEVs following a representative set of daily driving cycles. We use a mid-size power-split PHEV model to evaluate the energy costs associated with the drive cycles, and a high-fidelity battery model to examine PHEV battery degradation. The drive cycles are generated based on the travel data provided by the National Household Travel Survey (NHTS), plus the speed statistics of a set of federal and real-world drive cycles. We obtain aggregate PHEV power demand by accumulating the individual optimal PHEV charge patterns. Results indicate that the main PHEV peak load occurs early in the morning with nearly 45%-60% of PHEVs simultaneously charging. Moreover, charging at work can introduce additional peaks to this load.

The remainder of this paper is organized as follows: In Section 2 we develop a set of representative synthetic trips using the NHTS data and a Markov chain model for the PHEV velocity. In section 3, the PHEV model and the battery model are introduced, and the charge pattern optimization problem is formulated. Section 4 accomplishes the prediction of PHEV power demand, and Section 5 summarizes the paper's key conclusions.

2. SYNTHETIC TRIP GENERATION

In this section, we generate a set of representative synthetic trips for a population of PHEVs. This process is carried out in three steps. First, a set of representative trip start times, end times, and lengths is re-sampled from the statistical distributions of the National Household Travel Survey (NHTS) dataset. Second, a discrete-time Markov chain model is developed and trained for on-road vehicle velocity generation using a set of federal and real-world drive cycles. Third, the re-sampled NHTS data are integrated with the velocity profiles produced by the Markov chain model to obtain a set of representative daily PHEV trips.

Travel Data

We adopt the required travel information for PHEVs from the NHTS dataset which includes a large pool of data representing the driving behavior of American public, such the time, the length, and the purpose of various daily trips [16]. The purposes of the trips have been classified in different categories such as work-related, family/personal business, school/church, and etc. In this effort, we only focus on the work-related travels which include two trips a day, i.e., from home to work and vice versa. One of our goals is to estimate the extent to which PHEVs benefit by charging at work, and predict the corresponding grid load.

Among the NHTS available travel records for about 150,000 different drivers in the year 2001, we choose the statistics of nearly 8,500 drivers who commuted between home and work using cars (there are other means of transportation such as bus or subway which are not included in this study). Figure 1 shows the histograms of the first trip start time, the second trip start time, and the trip length, noting that the distribution of the first trip length and the second trip length are nearly identical. As seen, the peak values of the departure times are between 6:00 to 7:00 a.m. for the first trip (home to work), and 5:00 to 6:00 p.m. for the second trip (back home). Moreover, the peak value of the trip length distribution belongs to the range of 5 to 10 miles.

Since the size of the selected data is enormous for PHEV charge pattern optimization, we re-sample the NHTS data to generate a smaller set of representative trips (i.e., 20 trips) from the distributions shown in Figure 1. With 20 representative trips, we can complete the optimizations in reasonable computational time, while still capturing the key statistics of aggregate grid load.

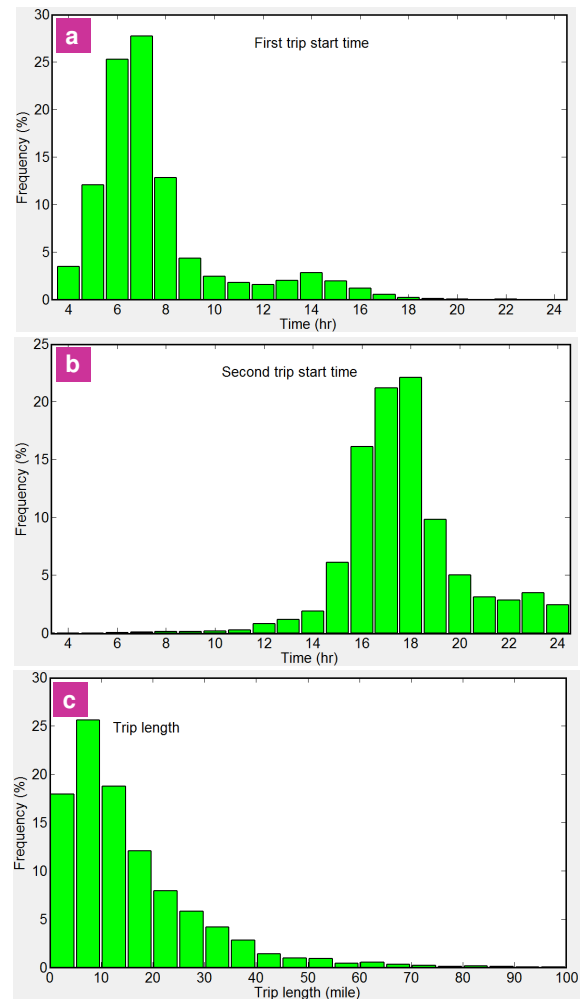


FIGURE 1. HISTOGRAMS OF (A) FIRST TRIP (HOME TO WORK) START TIME, (B) SECOND TRIP (WORK TO HOME) START TIME, AND (C) TRIP LENGTH.

Table 1 summarizes a statistical analysis performed to examine the correlation between selected variables from the NHTS data. As seen, the first and the second trips are very strongly correlated in length (correlation coefficient of 0.99), and strongly correlated in start time (correlation coefficient of 0.68). The correlations between the trip start times and the trip lengths are, however, weak. Therefore, we match the re-sampled data in a way that maximizes the correlation between the trip start times, but minimizes the correlation between the trip length and the trip start times. The latter is accomplished using a minimum-correlation Latin hypercube selection procedure [17]. Table 2 presents the timing and the length of the final 20 trips re-sampled from the NHTS distributions through this process.

TABLE 1. CORRELATION COEFFICIENTS BETWEEN THE VARIABLES SELECTED FROM THE NHTS DATASET.

	First trip start time	First trip length	Second trip start time	Second trip length
First trip start time	1.00	-0.17	0.68	-0.16
First trip length	-0.17	1.00	-0.01	0.99
Second trip start time	0.68	-0.01	1.00	-0.01
Second trip length	-0.16	0.99	-0.01	1.00

TABLE 2. SCHEDULE AND LENGTH OF 20 GENERATED TRIPS BASED ON ABOUT 8500 NHTS DRIVING DATA.

Trip #	First trip start time	Second trip start time	Trips length (mile)
1	4:35	12:07	11.47
2	5:17	14:13	10.00
3	5:36	14:57	7.83
4	5:57	15:14	24.36
5	6:08	15:19	1.26
6	6:24	15:49	9.02
7	6:30	16:01	6.00
8	6:40	16:15	6.90
9	6:55	16:18	20.76
10	7:01	16:40	28.49
11	7:14	17:00	14.53
12	7:27	17:03	15.80
13	7:32	17:15	18.36
14	7:47	17:22	3.09
15	8:01	18:00	5.03
16	8:24	18:18	53.28
17	9:03	19:10	34.94
18	10:33	20:31	12.50
19	13:18	22:10	2.17
20	15:36	24:31	4.29

Velocity Data

The velocity profiles for the trips described in Table 2 are generated from a Markov chain model of drive cycle behavior.

This model maps power demand-velocity pairs to a probability distribution over power demand in the next time step according to the following relationship:

$$P_{ijm} = \Pr(P_{dem,k+1} = j | P_{dem,k} = i, v_k = m) \quad (1)$$

where P_{dem} and v are respectively the power demand and velocity of the vehicle. The transition probabilities P_{ijm} are identified from a set of certification cycles (FTP-72, US06, HWFET) and real-world micro trips (WVUCITY, WVUSUB, WVUINTER) from the ADVISOR database [18] via maximum likelihood estimation procedure [19]. To generate velocity profiles from power demand we solve the following nonlinear equation for acceleration dv/dt and integrate over time:

$$P_{dem} = m \frac{dv}{dt} v + \frac{1}{2} \rho A_{fr} C_d v^3 + \mu mgv + b_w v^2 / r_{tire} \quad (2)$$

The right-hand side terms of Eq. (2) represent power demand due to vehicle acceleration, viscous air drag, rolling friction, and wheel damping, respectively. The trip length of these drive cycles are randomly generated from the distribution provided in Figure 1c.

Figure 2 depicts a sample velocity profile generated for the first part of Trip #10 of Table 2, with the length of 28.49 miles and a start time of 7:01 a.m. Figure 3 depicts all of the 20 representative drive cycles generated through the above procedures.

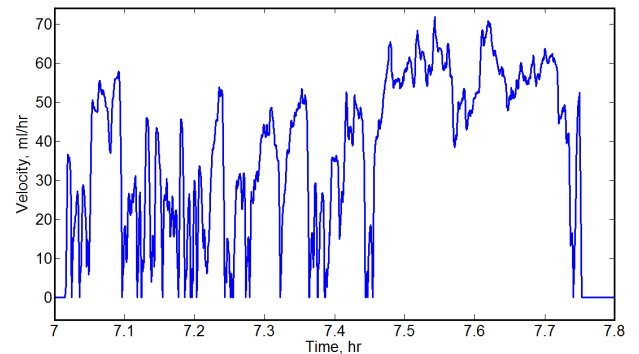


FIGURE 2. A SAMPLE VELOCITY PROFILE GENERATED FOR THE FIRST PART OF TRIP #10 OF TABLE 2.

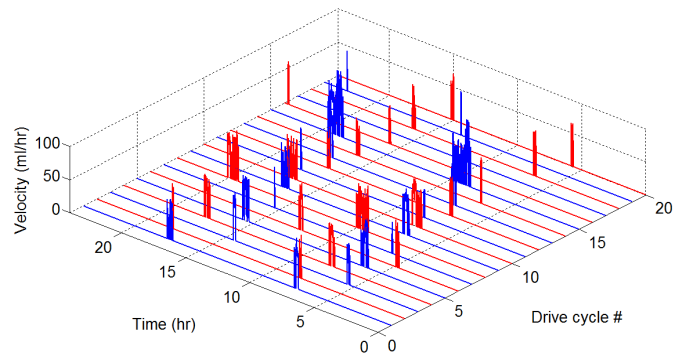


FIGURE 3. REPRESENTATIVE DRIVE CYCLES GENERATED USING THE NHTS DATA DISTRIBUTIONS AND THE MARKOV CHAIN MODEL.

3. PHEV CHARGE PATTERN OPTIMIZATION

The above drive cycles are used in a multiobjective genetic algorithm along with a PHEV model and a high-fidelity Li-ion battery model to optimize the charge pattern of PHEVs². The optimization objective is to simultaneously minimize (i) the total energy cost (fuel plus electricity), and (ii) the total battery degradation for the generated drive cycles. The first objective is calculated using a previously-developed stochastic optimal PHEV power management strategy [5], whereas the second objective is evaluated through an electrochemistry-based model of anode-side resistive film formation in Li-ion batteries [13-15]. We use a non-dominated sorting genetic algorithm, NSGA-II [20], for multiobjective optimization. This section briefly reviews the PHEV model and the battery model and their application in the PHEV charge pattern optimization problem.

PHEV Model with Optimal Power Management

The PHEV model used in this effort is based on a power-split mid-size sedan, similar in configuration and design to the 2002 Toyota Prius, with 12 kWh battery size. The supervisory power management algorithm, which determines the optimal split of engine and battery power, is developed using stochastic dynamic programming (SDP). We summarize the PHEV model and associated optimal supervisory control strategy here for comprehensiveness, but more details can be found in Ref. [5].

Figure 4 presents a conceptual map of the key interactions between the PHEV, the drive cycle, and the supervisory power management algorithm. The supervisory power management algorithm attempts to meet drive cycle power demand by adjusting three control inputs: engine torque, electric motor/generator 1 (M/G1) torque, and M/G2 torque. These inputs are determined by a nonlinear static feedback law, which depends functionally on engine speed, vehicle velocity, battery pack state-of-charge (SOC), and drive cycle power demand.

The vehicle model consists of five components shown schematically in Figure 4: the engine, motor/generators, planetary gear set, longitudinal vehicle dynamics, and battery pack. The engine and motor/generator models are steady-state maps that respectively output fuel consumption rate and power efficiency as functions of speed and torque. The drive cycle is modeled as a first order Markov process. Models for the remaining components can be grouped in terms of the inertial dynamics, road loads, and battery SOC dynamics. The inertial dynamics form state equations for the speeds of the engine, M/G1, and M/G2 (directly proportional to vehicle velocity). These three speeds must satisfy a kinematic constraint created by the planetary gear set. The road loads represent forces acting against the PHEV's inertia, including rolling resistance, viscous air drag, and wheel/axle bearing friction. For the purposes of control optimization, the battery pack is idealized by an open circuit voltage in series with an internal resistance. The battery pack SOC dynamics are determined by integrating battery current.

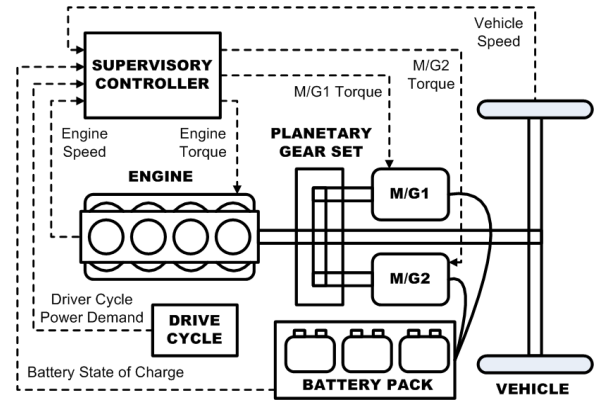


FIGURE 4. PHEV MODEL COMPONENTS, SUPERVISORY CONTROLLER, AND SIGNAL FLOW. NOTE THAT THE SIGNAL FLOW FORMS A STATE FEEDBACK CONTROL ARCHITECTURE.

The objective of the supervisory on-road power management algorithm is to minimize the expected consumption cost of both fuel (from the gas pump) and electricity (from the grid) over a stochastic distribution of drive cycles. This optimization is subject to the PHEV model dynamics, limits on the PHEV state and control signals, and a power conservation constraint that ensures the power sources continuously meet drive cycle power demand. The result is the supervisory control algorithm carefully blends engine and battery power when the battery pack SOC is greater than 25%. As the battery pack SOC approaches 25%, the algorithm enters a charge sustenance mode that maintains the SOC above 25% by operating similar to a conventional HEV. That is, the vehicle depletes battery energy when it is advantageous (low speeds and power demands), but regenerates SOC during other periods to maintain a relatively constant charge level. It is important to note that the supervisory on-road power management algorithm is explicitly designed to minimize an average energy consumption cost, but does not take into account factors that cause battery pack degradation. These two factors, energy consumption cost and battery pack aging, are the subject of the remainder of this paper.

Given a velocity profile and an initial battery SOC, the model can produce the trajectories of fuel and electricity consumption costs over time. Figure 4 depicts a preliminary simulation result of the developed PHEV model with optimal power management strategy. It shows the final values of energy consumption costs for the first part of Trip #10 (shown in Figure 2) as functions of the initial battery SOC (Fuel and electricity prices are chosen based on the average rates of year 2008 in the United States). As seen, the electricity cost increases with the increase of the initial battery SOC, but the fuel cost and more importantly, the total energy cost decrease with it. Charging the battery above 80% does not reduce the final energy cost any further extent since the provided trip does not require further electric energy. Thus, we can conclude that to minimize the total energy cost for a given trip, we must add sufficient charge to the battery for that trip. In the next section we examine the effects of battery SOC on its health degradation.

² Interested readers are encouraged to review Ref. [12] for more details of PHEV charge pattern optimization.

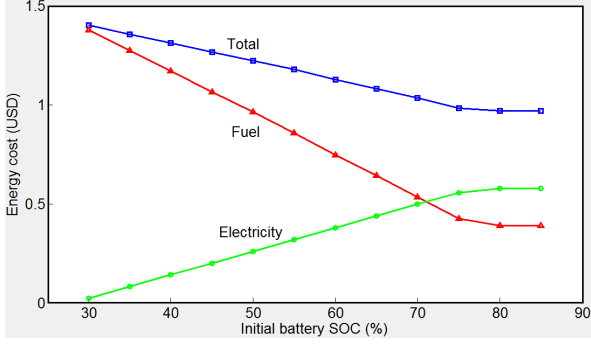


FIGURE 5. FUEL, ELECTRICITY, AND TOTAL ENERGY COSTS VERSUS INITIAL BATTERY SOC FOR THE FIRST PART OF TRIP #10.

Lithium-ion Battery Model

Li-ion batteries store electric energy by shuffling lithium ions between low and high potential energy states via a set of electrochemical processes. Lithium ions have the lowest energy when they are in the positive electrode (cathode) and the highest energy when they are in the negative electrode (anode). During charging, external current forces lithium ions to move from the cathode to the anode. During discharge, ions naturally move from the anode to the cathode, creating a useful current. Lithium ions movement is governed by two diffusion processes, as well as two electrochemical reactions driven by overpotentials. These electrochemical reactions allow the lithium ions to transfer between solid and solution phases via intercalation currents.

The battery model used in this effort is based on a first-principles electrochemistry model accounting for battery degradation [13]. The degradation mechanism is based on a side intercalation reaction occurring in the battery negative electrode (anode), resulting in the loss of lithium ions and the formation of an irreversible solid electrolyte interface (SEI) film. Based on the model, the governing equations of solid phase and solution phase potentials (represented by ϕ_1 and ϕ_2 , respectively) are given by Ohm's law as follows³:

$$\nabla \cdot (\sigma_j^{eff} \nabla \phi_{1,j}) - J = 0, \quad j = n, p \quad (3)$$

$$\nabla \cdot (\kappa^{eff} \nabla \phi_2) + \nabla \cdot (\kappa_D \nabla \ln(c_2)) + J = 0 \quad (4)$$

where σ_j^{eff} is the effective conductivity of electrode j (where n stands for the negative electrode and p for the positive electrode); κ^{eff} and κ_D represent the concentration-dependent effective and diffusional conductivities of the solution phase; $J = J_1 + J_{sd}$ is the total intercalation current density calculated from the Butler-Volmer expression for the main intercalation reaction current density given by:

$$J_1 = a_j i_{0,j} \left[\exp\left(\frac{\alpha_{a,j} F}{RT} \eta_j\right) - \exp\left(-\frac{\alpha_{c,j} F}{RT} \eta_j\right) \right], \quad j = n, p \quad (5)$$

³ List of all parameter values and the boundary conditions for the partial differential equations can be found in [15].

where

$$i_{0,j} = k_j (c_{1,j}^{max} - c_{1,j}^S)^{\alpha_{a,j}} (c_{1,j}^S)^{\alpha_{c,j}} (c_2)^{\alpha_{a,j}}, \quad j = n, p \quad (6)$$

and a side intercalation reaction current density governed by:

$$J_{sd} = -i_{0,sd} a_n \exp\left(-\frac{\alpha_{c,n} F}{RT} \eta_{sd}\right) \quad (7)$$

In these equations, a and k are the specific area of the porous electrode and the rate constant of electrochemical reaction, respectively; α_a and α_c are the anodic and cathodic transfer coefficients of the electrochemical reaction; F , R , and T respectively denote the Faraday's constant, universal gas constant and the temperature; c_1 and c_1^{max} represent the lithium concentration in the solid phase, and its maximum limit; i_0 and $i_{0,sd}$ are the exchange current densities for the main and the side reactions, respectively, and η and η_{sd} are the corresponding overpotentials, given by:

$$\eta_j = \phi_1 - \phi_2 - U_{ref,j} - \frac{J}{a_n} R_{film}, \quad j = n, p \quad (8)$$

$$\eta_{sd} = \phi_1 - \phi_2 - U_{ref,sd} - \frac{J}{a_n} R_{film} \quad (9)$$

where $U_{ref,j}$ is the SOC-dependent local equilibrium potential of the main reaction, R_{film} is the side film resistance in anode, and $U_{ref,sd}$ is the equilibrium potential for the side reaction.

In the solution phase, lithium ions are governed by a diffusion law combined with an intercalation current density term transferring ions between the solution and the solid:

$$\varepsilon_2 \frac{\partial c_2}{\partial t} = \nabla \cdot (D_2^{eff} \nabla c_2) + \frac{1-t^+}{F} J \quad (10)$$

where ε_2 represents the volume fraction of the solution phase, D_2^{eff} denotes the effective diffusion coefficient of lithium in the solution phase, and t^+ stands for the transference number.

The solid phase concentration is governed by a radially symmetric spherical diffusion process:

$$\frac{\partial c_{1,j}}{\partial t} = \frac{D_{1,j}}{r^2} \frac{\partial}{\partial r} \left(r^2 \frac{\partial c_{1,j}}{\partial r} \right) \quad (11)$$

where D_1 is the diffusion coefficient of lithium in the solid phase, and r is the sphere radius. This occurs at every point in anode and cathode, and is connected to the solution via the intercalation current density.

Finally, a resistive film builds up in anode as a result of side reaction:

$$\frac{\partial \delta_{film}}{\partial t} = -\frac{J_{sd} M_p}{a_n \rho_p F} \quad (12)$$

with δ_{film} being the thickness of the resistive film, and M_p and ρ_p representing the molecular weight and density of the side reaction

product, respectively. This results in the resistance increase of the side film as follows:

$$R_{film} = R_{SEI} + \frac{\delta_{film}}{K_p} \quad (13)$$

where R_{SEI} denotes the initial solid/electrolyte interface resistance, and K_p represents the conductivity of the side reaction product, respectively. The growth of the resistive film corresponds to the loss of cyclable lithium ions and therefore battery capacity fade.

To demonstrate the battery degradation process, we summarize the model's simulation in a 3D degradation map. Figure 6 shows this map obtained by simulating a reduced version of the battery model proposed in [15]. The map depicts the battery degradation rate in a SOC range of 5% to 85% and a charging rate of $-2C$ to $2C$, with negative sign indicating discharge. C -rate is a standard unit for battery charge and discharge, representing the ratio of the applied current (in Amp) to the rated capacity of battery (in Amp-hr). To obtain the map, we initialized the battery SOC at different levels through initializing the concentration of lithium ions in the electrodes, applied input currents at different rates to charge and discharge the battery, and then monitored the *average* resistance growth rate in the anode at the first step of the simulation.

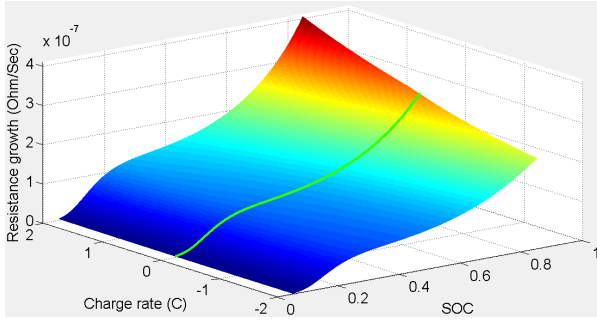


FIGURE 6. BATTERY DEGRADATION MAP.

From the degradation map, we see that at higher SOC's and higher charge rates the battery degrades faster. One of the particular cases of interest which is highly important in the PHEV charge pattern optimization problem is the energy storage application, in which battery maintains a constant level of charge while being at rest. This corresponds to the zero charge rate highlighted on the degradation map in Figure 6. We can see that a substantial degradation can still take place during energy storage, particularly at high SOC's. It is important to note that this SOC-dependent degradation trend of the model is consistent with the empirical trends available in the Li-ion battery literature [21, 22]. In the next section, we will examine the impact of battery degradation on the optimal PHEV charge patterns.

PHEV Charge Pattern Optimization

In this section, we carry out the PHEV charge pattern optimization for energy cost and battery health [12]. We assign variables including “the time”, “the maximum amount”, and “the rate” with which PHEVs receive charge before each trip. The

constant-current-constant-voltage (CC-CV) charging strategy is adopted, and a SOC cap of 85% is imposed on the battery. For a drive cycle with N separate trips the optimization objective is to:

$$\begin{aligned} & \text{Minimize}_x \left\{ \begin{aligned} & f_1(x) = \int_{24hr} J_{fuel}(x,t) dt + \int_{24hr} J_{elec}(x,t) dt \\ & \& (f_2(x) = \bar{R}_{film}^{24hr}(x)) \end{aligned} \right\} \\ & x = [x_1, x_2, x_3, \dots, x_{3N}] \\ & x_{3i-2}, i = 1, 2, \dots, N \text{ (i.e. } x_1, x_4, \dots, x_{3N-1}) \quad (14) \\ & \quad \text{charge start time for trip } i \\ & x_{3i-1}, i = 1, 2, \dots, N \text{ (i.e. } x_2, x_5, \dots, x_{3N-1}) \\ & \quad \text{charge rate for trip } i \text{ (between 0 and } 1C) \\ & x_{3i}, i = 1, 2, \dots, N \text{ (i.e. } x_3, x_6, \dots, x_{3N}) \\ & \quad \text{charge amount for trip } i \text{ (up to 85\% SOC)} \end{aligned}$$

where J_{fuel} and J_{elec} are the instantaneous fuel and electricity dollar costs per unit time, \bar{R}_{film}^{24hr} is the final resistance growth of the anode-side film at the end of the 24-hr simulation, and x is the vector of optimization variables defining the PHEV charge patterns. The upper and lower bounds of the variables associated with the charge times are set to cover the entire time span between the trips. The fuel consumption cost, J_{fuel} , is calculated from the optimal blending power management strategy proposed in Ref. [5] and explained earlier in the paper. The electricity price during the day consists of two different rates: during the on-peak hours (10.00 am until 7.00 pm) the electricity rate is 0.099 USD/kWh, while during the off-peak hours this rate reduces to 0.035 USD/kWh. This pricing policy has been taken from the DTE Energy website for electric vehicles within the period of June to September 2009 [23].

Two PHEV charging scenarios are examined. First we constrain the PHEVs to charge at home only, and then we allow them to charge both at home and at work. Therefore, for the first scenario, the optimization problem consists of three variables, whereas in the second scenario, six variables are included (three for each trip). We use NSGA-II [20] for the multiobjective optimization problem introduced in this section.

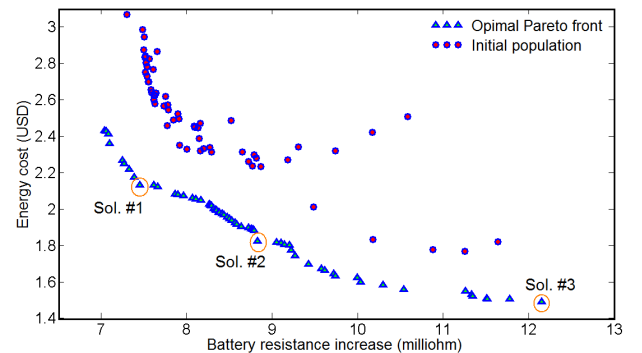


FIGURE 7. SAMPLE PHEV CHARGE PATTERN OPTIMIZATION FOR THE DRIVE CYCLE #10.

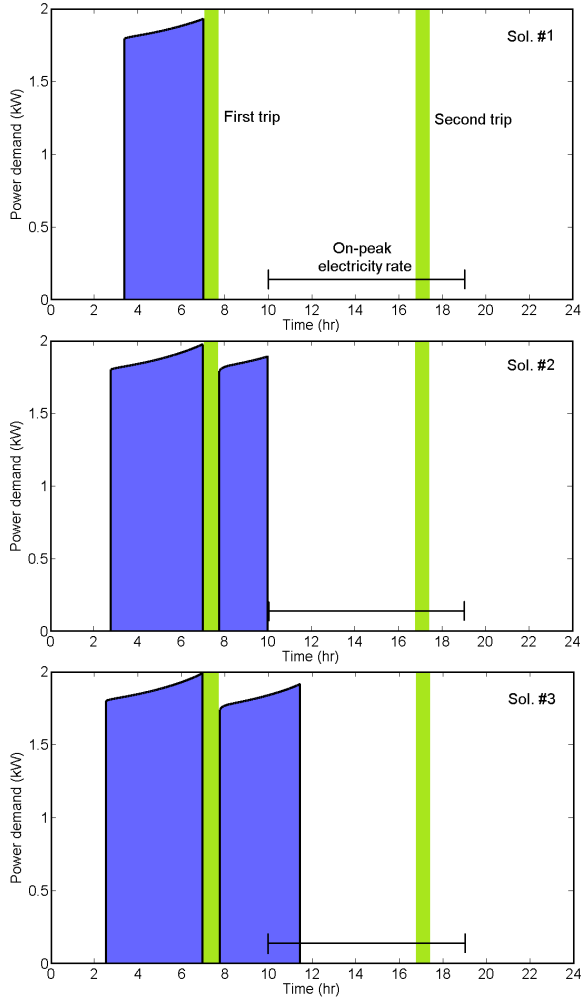


FIGURE 8. THREE SAMPLE CHARGE PATTERNS FROM THE OPTIMAL PARETO FRONT SHOWN IN FIGURE 7.

Figure 7 depicts the optimization result for the drive cycle #10, for the second charging scenario (i.e., charging at home and at work). After 50 generations of 60 members, the genetic algorithm results in an optimal Pareto front as shown in Figure 7. Each solution in the Pareto front corresponds to an optimal charge pattern. To illustrate the difference between them, we select three sample solutions (i.e., Solutions #1-3) and show their corresponding charge patterns in Figure 8. As seen, there is only one charging event in Sol. #1, even though a second charging is also allowed. In Sol. #2, the second charging terminates right before the electricity price jumps to the on-peak rate. In Sol. #3, the second charging continues during the on-peak hours until sufficient electric energy is stored in the battery. The optimal charge rate in all cases is close to the maximum rate of 2 kW which is chosen based on the regular residential power limits. The slow increase of the battery power during charging is due to the gradual increase of battery voltage during charging.

In all solutions, the first charging event is delayed until before the start of the first trip. This is dictated by the battery degradation dynamics discussed earlier in the paper. The delayed charging for

the second trip in Figure 8 is, however, limited by the electricity price jump. Obviously, if the electricity price was entirely flat, the second charging would be also delayed until before the start of the second trip.

In the next section, we will accomplish the battery health-conscious PHEV power demand prediction using the optimal charge patterns obtained for all of the 20 generated drive cycles.

4. PREDICTION OF PHEV POWER DEMAND

We obtain the aggregate PHEV power demand by choosing and accumulating the individual charge patterns from the Pareto fronts obtained for the examined drive cycles. To select the charge patterns, we apply a secondary optimization in which a weighted summation of the objective functions in the Pareto front is minimized. This procedure is discussed next.

Charge Pattern Selection for Power Demand Prediction

To select a charge pattern from the Pareto front, we minimize a weighted sum of normalized objective functions, i.e., $f_{1n} + \alpha f_{2n}$, where f_{1n} and f_{2n} are the normalized functions corresponding to resistive film growth in battery and total energy cost, respectively. The normalization is carried out by dividing the objective function values by their mean values in the Pareto front. The weighing coefficient, α , determines the importance of energy cost reduction versus battery health degradation. For example, the charge patterns shown in Figure 8 (Solutions #1-3) correspond to α values of 0.2, 1, and 5, respectively. Small values of α correspond to less battery degradation whereas large α 's result in less energy cost. We will choose various values for α to assess the effects of this parameter on the aggregate PHEV power demand.

Prediction of Aggregate PHEV Power Demand

We obtain the aggregate PHEV power demand by choosing a charging scenario and a value for α , and then accumulating the individual charge patterns. Figures 9 and 10 depict the battery health-conscious PHEV grid power demand predictions. The most important observations from these results are summarized as follows:

- The main load peak occurs between 5:00-6:00 a.m. for all of the examined cases.
- There is a secondary peak around 8:00 a.m. (smaller than the first peak) for some of the investigated cases when charging at work is applied. This peak is due to the jump in the electricity price at 10:00 a.m.
- There is sudden drop in the load at 10:00 a.m. when charging at work is applied.
- There is a third peak between 4:00-5:00 p.m., smaller than the first and the second peak, if charging at work is applied.
- During the peak load, 45% to 60% of PHEVs receive electricity from the grid (depending on the charging scenario and the value of weighing parameter).

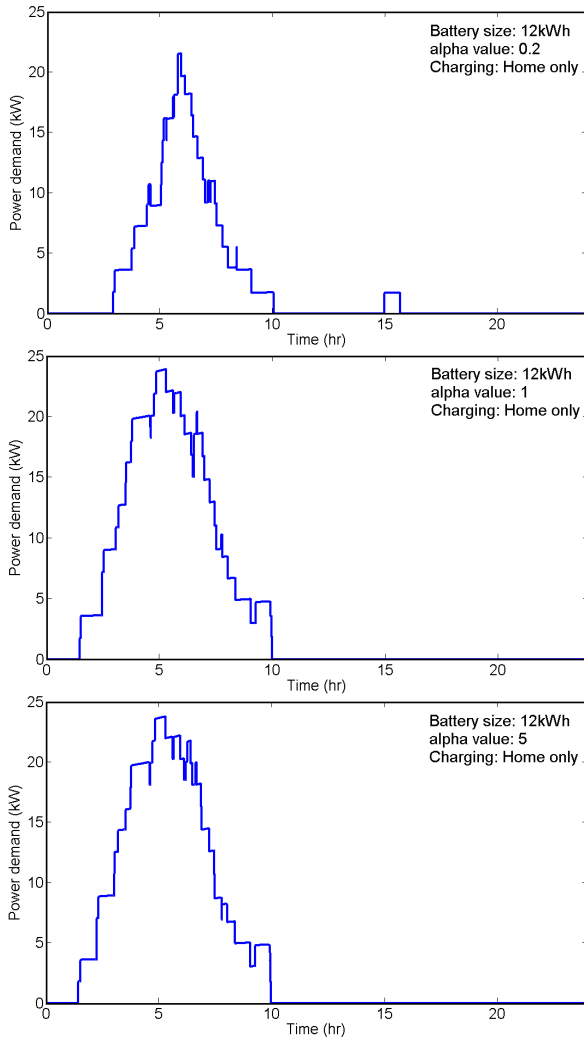


FIGURE 9. BATTERY HEALTH-CONSCIOUS PHEV POWER DEMAND PREDICTION (CHARGING AT HOME ONLY).

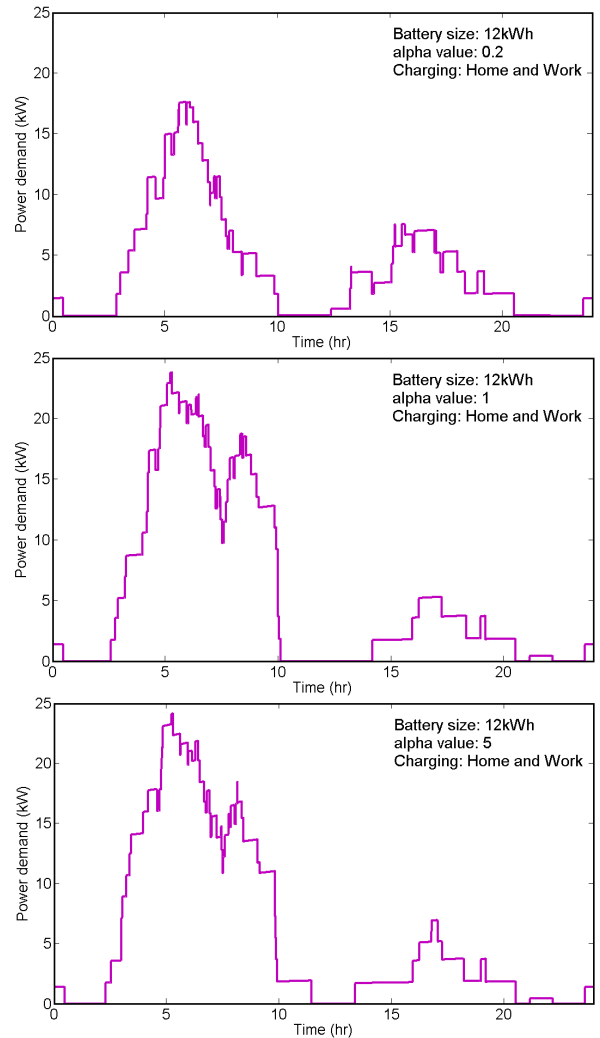


FIGURE 10. BATTERY HEALTH-CONSCIOUS PHEV POWER DEMAND PREDICTION (CHARGING AT HOME AND WORK).

The results obtained in this paper are based on a particular PHEV configuration, a given pricing policy, a set of specific trips (i.e., work related trips), a specific model of battery health degradation, and finally, the assumption that consumers will adopt the developed battery health-conscious charging policies. However, the methods proposed herein can be used to analyze PHEV grid loads under other optimization scenarios. Key factors for consideration in future PHEV grid load studies include electricity pricing, real-time load management, and full vehicle-to-grid (V2G) integration with bidirectional power flow.

5. SUMMARY AND CONCLUSIONS

This paper examined the problem of predicting the aggregate grid load imposed by the battery health-conscious charging of plug-in hybrid electric vehicles (PHEVs). The paper modeled a representative PHEV powertrain, and utilized previous stochastic dynamic programming (SDP) research by the authors to optimize its on-road power management for total energy cost. The paper

then used an electrochemistry-based lithium-ion battery model to predict the PHEV’s battery health degradation over the course of a full daily drive cycle. Twenty representative sets of daily trip start times and trip lengths were re-sampled from the statistics of the NHTS database. For each of these sample trips, on-road vehicle velocity was generated as a function of time using a Markov chain model trained on both federal and naturalistic driving data. For each of the resulting daily trip descriptions, we used NSGA-II to obtain a Pareto set of PHEV charge patterns optimizing both total PHEV energy cost and battery health. Aggregating the resulting PHEV charge patterns furnished a prediction of the battery health-conscious PHEV grid load. Unlike the PHEV-induced grid loads traditionally studied in the literature, our results show a peak load early in the morning (between 5.00am-6.00am), immediately preceding departure to work. Moreover, if charging at work is provided, there are secondary and tertiary peaks as well, smaller than the first peak. During the peak load at 2kW charge rate, approximately 45% to 60% of the PHEV population receives electricity from the grid.

ACKNOWLEDGMENTS

This research was supported by a research partnership led by the University of Michigan and DTE Energy, and funded by a Michigan Public Service Commission Grant. The authors gratefully acknowledge this support.

REFERENCES

- [1] D. Wu and D. Aliprantis, "Impacts of PHEV on electric power system", Presentation for NETSCORE 21, February 2009.
- [2] S. Hadley and A. Tsvetkova, "Potential impacts of Plug-in Hybrid Electric Vehicles on regional power generation", ORNL/TM report, January 2008.
- [3] S. J. Moura, D. S. Callaway, H. K. Fathy, and J. L. Stein, "Tradeoffs between battery energy capacity and stochastic optimal power management in plug-in hybrid electric vehicles," *Journal of Power Sources*, in press.
- [4] A. Emadi, Y. J. Lee, and K. Rajashekara, "Power electronics and motor drives in electric, hybrid electric, and plug-in hybrid electric vehicles," *IEEE Transactions on Industrial Electronics*, 55, pp 2237-2245, 2008.
- [5] S. J. Moura, H. K. Fathy, D. S. Callaway, J. L. Stein, "A stochastic optimal control approach for power management in plug-in hybrid electric vehicles," *Proceedings of the 2008 ASME Dynamic Systems and Control Conference*, Ann Arbor, MI, October 2008.
- [6] W. Kempton and J. Tomic, "Vehicle-to-grid power fundamentals: calculating capacity and net revenue," *Journal of Power Sources*, 144, pp. 268-279, 2005.
- [7] W. Kempton and J. Tomic, "Vehicle-to-grid power implementation: From stabilizing the grid to supporting large-scale renewable energy," *Journal of Power Sources*, 144, pp. 280-294, 2005.
- [8] C. Guille and G. Gross, "A conceptual framework for the vehicle-to-grid (v2G) implementation," *Energy Policy*, 37, pp. 4379-4390, 2009.
- [9] M. D. Galus and G. Andersson, "Demand management of grid connected plug-in hybrid electric vehicles (PHEV)," *IEEE Energy 2030 conference*, Atlanta, GA, November 2008.
- [10] J. T. B. A. Kessels, and P. P. J. V. D. Bosch, "Plug-in hybrid electric vehicles in dynamical energy markets," *2008 IEEE Intelligent Vehicles Symposium*, Eindhoven, The Netherlands, June 2008.
- [11] S. B. Peterson, J. Apt, J. F. Whitacre, "Lithium-ion battery cell degradation resulting from realistic vehicle, and vehicle-to-grid utilization," *Journal of Power Sources*, 2009 (available online).
- [12] S. Bashash, S. J. Moura, and H. K. Fathy, "Plug-in hybrid electric vehicles charge pattern optimization for energy cost and battery health," *Proceedings of the 2010 American Control Conference*, Baltimore, MD, June/July 2010.
- [13] P. Ramadass, B. Haran, P. Gomadam, R. White, and B. Popov, "Development of first principles capacity fade model for Li-ion cells," *Journal of Electrochemical Society*, 151, pp. 196-2003, 2004.
- [14] S. Santhanagopalan, Q. Guo, P. Ramadass, and R. White, "Review of models for predicting the cycling performance of Lithium ion batteries," *Journal of Electrochemical Society*, 156, pp. 620-628, 2006.
- [15] J. Forman, S. Bashash, H. K. Fathy, and J. L. Stein, "Reduction of an electrochemistry-based Li-ion battery health degradation model via constraint linearization and Padé approximation," *Proceedings of the 2010 ASME Dynamic Systems and Control Conference*, Cambridge, MA, September 2010.
- [16] U.S. DOT, National Household Travel Survey (<http://nhts.ornl.gov/>).
- [17] A. Owen, "Controlling correlations in Latin hypercube samples," *Journal of American Statistical Association*, 89, pp. 1517-1522, 1994.
- [18] W. B. Wipke, M. R. Cuddy and S. D. Burch, "ADVISOR 2.1: A user-friendly advanced powertrain simulation using a combined backward/forward approach," *IEEE Transactions on Vehicular Technology*, 48, pp. 1751-1761, 1999.
- [19] T. W. Anderson and L. A. Goodman, "Statistical inference about Markov chains," *Annals of Mathematical Statistics*, 28, pp. 89-110, 1957.
- [20] K. Deb, A. Pratap, S. Agarwal, and T. Meyarivan, "A fast and elitist multiobjective genetic algorithm: NSGA-II," *IEEE Transactions on Evolutionary Computation*, 40, pp. 181-197, 2002.
- [21] Ichimura M., Shimomura M., Takeno K., Shiota R., Yakami J., "Synergistic effect of charge/discharge cycle and storage in degradation of lithium-ion batteries for mobile phones," *27th International Conference on Telecommunications*, 245-250, 2005.
- [22] Jungst R. G., Nagasubramanian G., Case H. L., Liaw B. Y., Urbina A., Paez T. L., Doughty D. H., 2003. "Accelerated calendar and pulse life analysis of lithium-ion cells," *Journal of Power Sources*, 119, 870-873.
- [23] DTE Energy website, Residential Electric Rates: (<http://www.dteenergy.com/residentialCustomers/billing/Payment/rates/electric/resRates.html>).